Rigorous Field Theory Design of Millimeter-Wave *E*-Plane Integrated Circuit Multiplexers

JOACHIM DITTLOFF AND FRITZ ARNDT, SENIOR MEMBER, IEEE

Abstract—**The overall field theory designs of two types of quasi-planar millimeter-wave multiplexers utilizing low-cost, low-insertion-loss printed metallic *E*-plane filters are described. Very compact components are achieved by using *E*-plane filters printed on a common metal sheet which is directly integrated in the septate sections of an *E*-plane *n*-furcated split-block waveguide housing. The second configuration proposed extends the useful principle of waveguide *H*-plane slit-coupled manifold multiplexers to the case of millimeter-wave printed metallic *E*-plane filters. Based on the modal scattering matrix description of suitable key building blocks, the rigorous simulation technique used comprises the complete multiplexer structure including the *E*-plane transformer or iris elements, the waveguide *E*- or *H*-plane junctions, and the filter sections. The optimization process takes all relevant influences into account, such as finite metallization thicknesses and the higher order mode interactions of all discontinuities. Computer-optimized data are presented for seven-resonator metal insert filter diplexer and triplexer examples in the *E*-band (60–90 GHz) designed for common-port passband return losses of more than 25 dB and 20 dB, respectively. The theory is verified by measured results of typical individual components and of a septate *E*-plane diplexer realized in the *Ku*-band.**

I. INTRODUCTION

INCREASING progress in millimeter-wave receiver technology has created the need for compact, low-cost, high-performance diplexers and multiplexers utilizing quasi-planar printed-circuit components [1]–[10]. Previous designs use quadrature hybrid coupled *E*-plane dual low-pass [1] and bandpass filters [2]–[4], [8], or common junction *E*-plane tee [5], *H*-plane tee [4], [6], coaxial probe [7], and suspended probe coupling techniques [9], [10]. Hybrid and probe feeding methods require supplementary coupling structures, which may cause additional costs and losses [11], [12]; with open *H*-plane tee junctions it may be difficult to compensate for the rapid reactance variation [13].

This paper describes two new types of quasi-planar millimeter-wave multiplexer configurations (Fig. 1) which avoid these shortcomings and may help to take advantage of the full low insertion loss and low-weight potential inherent in the metallic *E*-plane filter technology. The directly fed multiplexer, recently introduced by the authors [27], is integrated in the septate waveguide *E*-plane (Fig. 1(a)) and hence combines the attributes of the compact, low-cost design of *E*-plane filters printed on a common metal sheet with the broad-band low-insertion-loss properties of *E*-plane *n*-furcated power dividers [14]. The manifold type (Fig. 1(b)) extends the known useful design principle of waveguide *H*-plane slit-coupled manifold multiplexers [17] to the case of quasi-planar metallic *E*-plane filters.

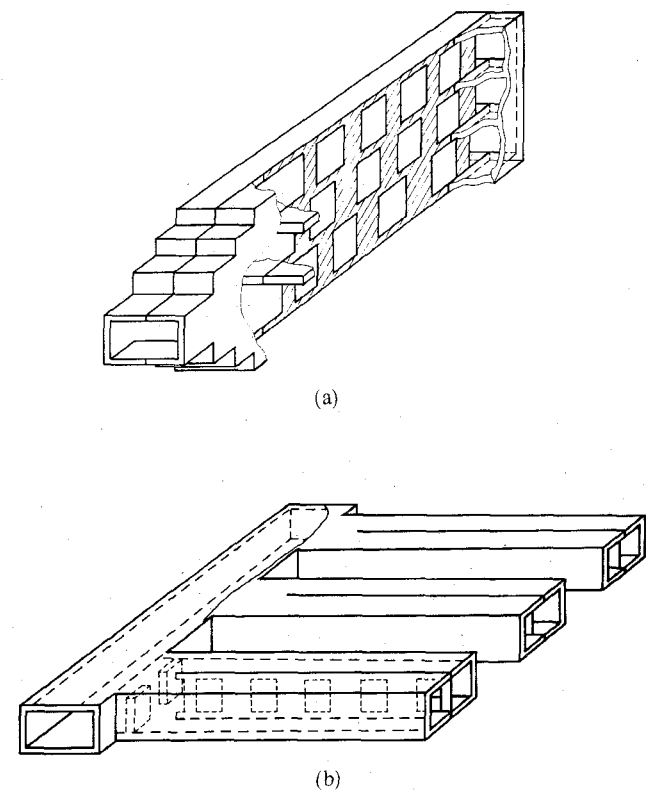

Fig. 1. Quasi-planar millimeter-wave *E*-plane integrated circuit multiplexers. (a) Septate *E*-plane multiplexer with metallic *E*-plane filters on a common metal sheet. (b) Waveguide *H*-plane slit-coupled manifold multiplexer with metallic *E*-plane filters.

Many refined design procedures are available based on impedance inverter and low-pass prototype techniques [11], [15]–[17], [2]–[4], [7], [8], on equivalent circuit methods [18], and on exact filter data combined with equivalent circuits for the junctions [6], [9], [10]. As higher order mode

Manuscript received January 14, 1988; revised July 21, 1988.

The authors are with the Microwave Department, University of Bremen, Kufsteiner St. NW1, D-2800 Bremen 33, West Germany.

IEEE Log Number 8824980.

0018-9480/89/0200-0340$01.00 ©1989 IEEE

interaction effects have turned out to be of increasing importance at millimeter-wave frequencies, even for designing single filters [19]–[22], rigorous methods must be applied for the reliable computer-aided design of the complete multiplexer structure. Moreover, it may be desirable to utilize the full design potential of the quasi-planar multiplexer technology, such as compactness and low cost, by using exact field theory methods in the optimization process, which take all mutual compensation effects of the individual multiplexer elements rigorously into account and hence may help to avoid extra immittance compensation networks.

The computer-aided design method in his paper, therefore, is based on field expansion into normalized eigenmodes [13], [14], [20], [22]–[25], which yield directly the modal S matrix of appropriate key building-block discontinuities. The immediate modal S matrix combination of all interacting structures includes the higher order mode coupling effects and the finite thickness or spacing of all obstacles and allows the stopband characteristics of the filters to be included in the multiplexer design. For computer optimization, the evolution strategy method [20], [22], [25], [26], i.e., a suitably modified direct search procedure, is applied where no differentiation step in the optimization process is necessary and hence the problem of local minima may be circumvented.

Design examples for optimized diplexers and triplexers in the E-band (60–90 GHz) are given. The septate E-plane and the manifold diplexers achieve calculated minimum common port passband return losses of about 25 dB; the values of the corresponding triplexers are about 20 dB. The theory is verified by measured results of the individual components (i.e., septate E-plane power divider, H-plane tee, and the metal insert filter), by comparison of the common-port scattering coefficients with the characteristic of the individual filters, and by measurements at a *Ku*-band diplexer prototype.

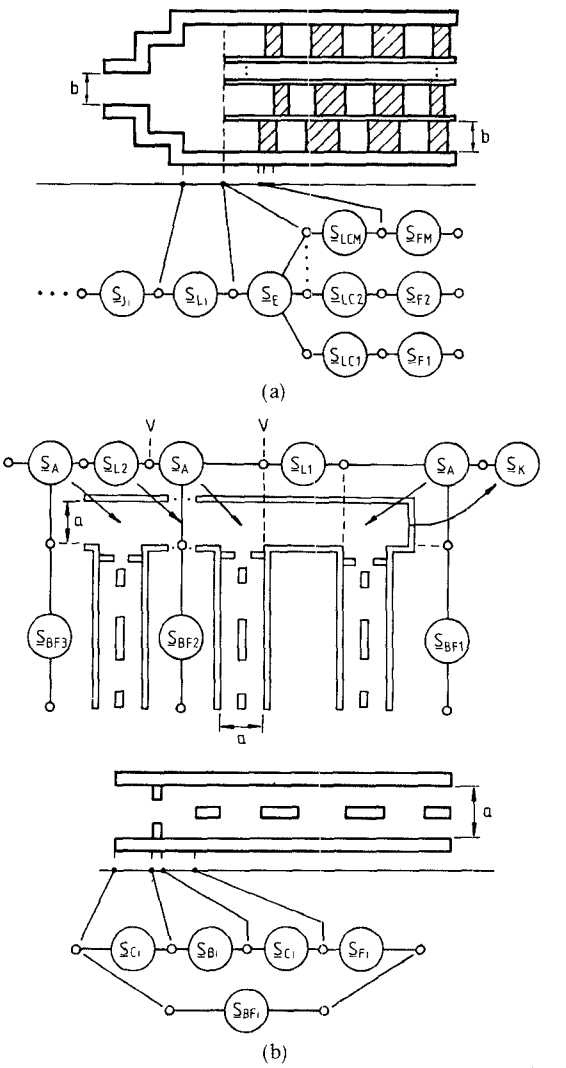

Fig. 2. Scheme for the calculation of the overall modal scattering matrix of the multiplexers. (a) Septate E-plane multiplexer. (b) H-plane slit-coupled manifold multiplexer, with the inductive iris slit-coupled metallic E-plane filters.

II. Theory

For the computer-aided design of the quasi-planar multiplexers (Fig. 1), the known modal S-matrix method is applied [14], [22], [24], [25]. For the field theory treatment, the complete actual multiplexer structure (Fig. 2(a) or (b), respectively) is decomposed into appropriate general *key building-block elements* (Fig. 3):

1) The *waveguide E-plane or H-plane n-furcation* (Fig. 3(a)). The E-plane n-furcation with the individual modal S matrix S_E (Fig. 2(a)) is utilized for the multiplexer type in Fig. 1(a) (for this case, the c expressions in Fig. 3(a) denote the waveguide b dimensions). The H-plane bifurcation (with $M = \text{II}$) is used for calculating the filter coupling sections (cf. Fig. 3(d); the c expressions denote the corresponding a dimensions).
2) The *abrupt change in waveguide height or width* (Fig. 3(b)). The change in height is utilized for the transformer section with the modal S matrix S_J in Fig. 2(a) (c in Fig. 3(b) denoting the b dimensions). The change in width is necessary for calculating the H-plane iris (Fig. 3(e)) with the matrix S_B (Fig. 2(b)) (c stands for the a dimensions).
3) The *H-plane tee* (Fig. 3(c)) with the matrix S_A (cf. Fig. 2(b)).

Combination with the known scattering matrices of the corresponding intermediate homogeneous waveguide sections S_L, S_C, S_{LC} (Fig. 2) yields the modal S matrices of related subelements, e.g. S_{BF} in Fig. 2(b). The overall scattering matrix of the total multiplexer is then calculated by a suitable direct combination of all single modal scattering matrices [14], [22], [24], [25].

Along the H-plane slit coupled manifold multiplexer (Figs. 1(b), 2(b)), only TE_{m0} modes are excited at the H-plane discontinuities [23]. For the septate E-plane multiplexer (Figs. 1(a), 2(a)), however, the direct combination of all individual structures (E-plane and H-plane step discontinuities), without any restrictions concerning their

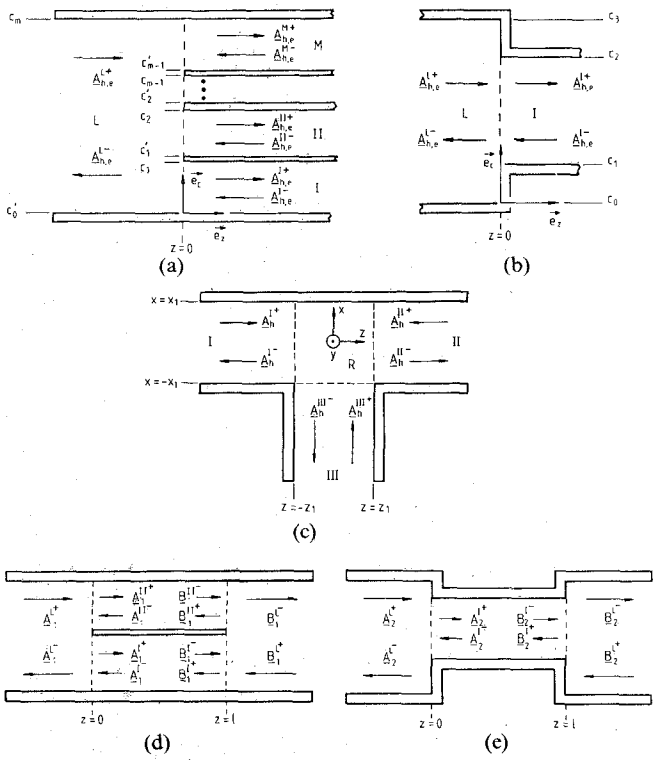

Fig. 3. Key building block elements, and complete filter coupling sections of finite lengths, for the calculation of the overall scattering matrix of the multiplexers. (a) General E- or H-plane n-furcation key building block. (b) Key building block of abrupt change in waveguide height or width. (c) H-plane tee key building block. (d) Metal strip coupling section of finite length. (e) H-plane iris coupling section of finite length.

mutual distance, requires all six field components to be considered, at each discontinuity. For the *general homogeneous waveguide subregion* under consideration, therefore, the fields [23]

$$\vec{E} = \frac{1}{j\omega\epsilon}\,\mathrm{rot}\,\mathrm{rot}\left(A_{ez}\vec{e}_z\right) + \mathrm{rot}\left(A_{hz}\vec{e}_z\right)$$

$$\vec{H} = -\frac{1}{j\omega\mu}\,\mathrm{rot}\,\mathrm{rot}\left(A_{hz}\vec{e}_z\right) + \mathrm{rot}\left(A_{ez}\vec{e}_z\right) \qquad (1)$$

are derived from the z components of the magnetic (h) and electric (e) vector potentials

$$A^o_{ez} = \sum_{i^o} Q^o_{i^o} T^o_{e_{i^o}} \left(A^{o\pm}_{e_{i^o}} e^{\mp jk^o_{ze_{i^o}} z} \right)$$

$$A^o_{hz} = \sum_{i^o} Q^o_{i^o} T^o_{h_{i^o}} \left(A^{o\pm}_{h_{i^o}} e^{\mp jk^o_{zh_{i^o}} z} \right) \qquad (2)$$

where $o = 1,2,3,\cdots,M_s$ (M_s = total number of subregions), i^o is the index for all TE and TM modes in each subregion, Q denotes the normalization factors due to the complex power, and T represents the eigenfunctions in the corresponding subregions [14], [20], [22]–[25]. A denotes the amplitude coefficients of the forward (+) and backward (−) waves, and k_z represents the wavenumbers of the corresponding TE and TM modes [23]. For the special case of TE_{m0} mode excitation, the electric vector potential in (1) is chosen to be $A_{ez} = 0$.

By matching the tangential field components at the common interfaces at the individual step discontinuities, the wave amplitude coefficients of (2) can be related to each other after multiplication with the appropriate orthogonal function [14], [20], [22]–[25]. This yields the modal scattering matrices of the key building-block discontinuities in Fig. 3.

The relations for the *modal scattering matrix elements of the general E- and H-plane n-furcation* (Fig. 3(a)) are given by

$$\underline{A}^{L^-} = \underbrace{\underline{Y}\left(\sum_{k=I}^{M} \left(\underline{G}^{Lk}\underline{G}^{Lk'} \right) - \underline{E} \right)}_{\underline{S}_{LL}} \underline{A}^{L^+} + \underbrace{\sum_{k=I}^{M} \underline{Y}2\underline{G}^{Lk}}_{\underline{S}_{Lk}} \underline{A}^{k^-}$$

$$\underline{A}^{k^+} = \underbrace{\left(-\underline{G}^{Lk'}\underline{S}_{LL} + \underline{G}^{Lk'} \right)}_{\underline{S}_{kL}} \underline{A}^{L^+} + \underbrace{\left(\underline{E} - \underline{G}^{Lk'}\underline{S}_{Lk} \right)}_{\underline{S}_{kk}} \underline{A}^{k^-} + \qquad (3)$$

$$+ \underbrace{\sum_{u}^{M} -\underline{G}^{Lk'}\underline{S}_{Lu}}_{\underline{S}_{ku}} \underline{A}^{u^-}$$

where $\underline{Y} = (\underline{E} + \sum_{k=1}^{M} \underline{G}^{Lk}\underline{G}^{Lk'})^{-1}$ and $\underline{E}$ = unit matrix, k = I, II, III, $\cdots$, M (cf. Fig. 3(a)), u = I, II, III, $\cdots$, $M (u \neq k)$, and the elements $\underline{G}$ are elucidated in the Appendix. Note that only one matrix inversion is required for deriving the relations in (3).

The modal scattering matrix of a *general waveguide step discontinuity* (Fig. 3(b)) is already available [24], [25]. For deriving the equations of this key building block, the reader is therefore referred to the literature.

The relations for the modal scattering matrix of the key building-block *H-plane tee* (Fig. 3(c)) are given by

$$\begin{aligned}
\underline{A}_h^{\mathrm{I}^-} &= (\underline{M}_1\underline{N}_1 + \underline{M}_2)\underline{A}_h^{\mathrm{I}^+} + (\underline{M}_1\underline{N}_2 + \underline{M}_3)\underline{A}_h^{\mathrm{II}^+} \\
&\quad + (\underline{M}_1\underline{N}_3 + \underline{M}_1)\underline{A}_h^{\mathrm{III}^+} \\
\underline{A}_h^{\mathrm{II}^-} &= (\underline{M}_4\underline{N}_1 + \underline{M}_3)\underline{A}_h^{\mathrm{I}^+} + (\underline{M}_4\underline{N}_2 + \underline{M}_2)\underline{A}_h^{\mathrm{II}^+} \qquad (4) \\
&\quad + (\underline{M}_4\underline{N}_3 + \underline{M}_4)\underline{A}_h^{\mathrm{III}^+} \\
\underline{A}_h^{\mathrm{III}^-} &= \underline{N}_1\underline{A}_h^{\mathrm{I}^+} + \underline{N}_2\underline{A}_h^{\mathrm{II}^+} + \underline{N}_3\underline{A}_h^{\mathrm{III}^+}
\end{aligned}$$

where these elements also are elucidated in the Appendix.

For the *filter coupling section elements*, metal strip (Fig. 3(d)) and inductive iris (Fig. 3(e)), it is numerically more adequate to calculate the related modal scattering matrices of the complete section of finite length l directly by using the formulations of the corresponding key building-block elements instead of decomposing the structure into more

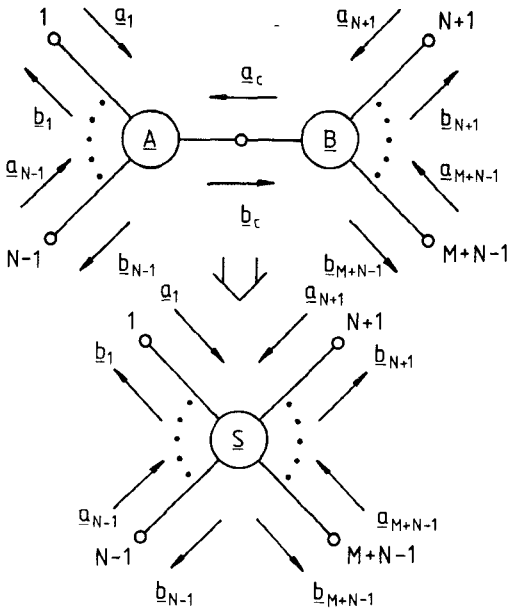

Fig. 4. Scheme for the general direct combination of the modal scattering matrices of two multiports.

possible subelements. The relations for the modal scattering matrix elements of the metal strip section (Fig. 3(d)) and the inductive iris section (Fig. 3(e)) of finite length l are given by

$$\underline{A}_i^{L^-} = \overbrace{\underline{V}(\underline{T}-\underline{E}-\underline{U}(\underline{E}+\underline{T})^{-1}\underline{U})}^{\underline{S}_{11_i}}\underline{A}_i^{L^+} + \overbrace{\underline{V}\underline{U}(\underline{E}-(\underline{E}+\underline{T})^{-1}(\underline{T}-\underline{E}))}^{\underline{S}_{12_i}}\underline{B}_i^{L^+}$$

$$\underline{B}_i^{L^-} = \underline{S}_{12_i}\underline{A}_i^{L^+} + \underline{S}_{11_i}\underline{B}_i^{L^+} \qquad (5)$$

where $i = 1,2$ denotes the elements of the strip section (Fig. 3(d)) or inductive iris section (Fig. 3(e)), respectively; $M = \text{II}$ (strip section), $M = \text{I}$ (iris section), and

$$\underline{Y}_l^k = \left(\underline{E} - \underline{L}_l^k\underline{L}_l^k\right)^{-1} \qquad \underline{E} = \text{unit matrix}$$

$$\underline{T}_l = \sum_{k=I}^{M} \underline{G}_l^{Lk}\left(\underline{Y}_l^k + \underline{L}_l^k\underline{Y}_l^k\underline{L}_l^k\right)\underline{G}_l^{Lk'}$$

$$\underline{U}_l = \sum_{k=I}^{M} \underline{G}_l^{Lk}\left(\underline{Y}_l^k\underline{L}_l^k + \underline{L}_l^k\underline{Y}_l^k\right)\underline{G}_l^{Lk'}$$

$$\underline{V}_l = \left(\underline{E} + \underline{T}_l - \underline{U}_l(\underline{E}+\underline{T}_l)^{-1}\underline{U}_l\right)^{-1}. \qquad (6)$$

The choice of the corresponding submatrix elements $\underline{G}$, which are elucidated in the Appendix, determines the mode excitation desired: TE_{m0} modes in the case of the manifold multiplexer and all TE and TM modes for the septate E-plane multiplexer.

In order to preserve numerical accuracy, a *direct combination of the modal scattering matrices* of all step discontinuities and of the intermediate homogeneous waveguide sections is used. The advantage of this procedure has

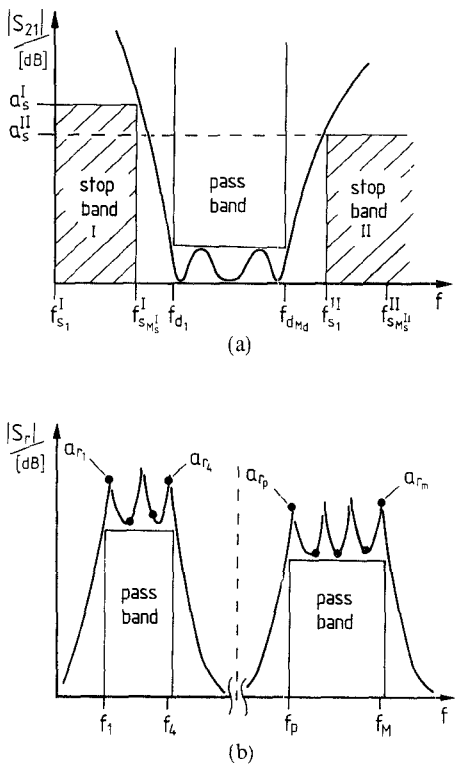

Fig. 5. Scheme for the computer optimization (cf. eqs. (8) and (9)). (a) Metallic E-plane filters. (b) Overall multiplexer including the filters.

already been demonstrated for two-ports (cf. [20], [22], [24], [25]). For the multiplexer structures considered in this paper (Fig. 2), the general relations, which may be used iteratively, combining the multiport modal scattering matrices $\underline{A}$ and $\underline{B}$ (Fig. 4), are given by

$$\underline{b}_k = \left(\sum_{i=1}^{N-1}\left(\underline{A}_{ki} + \underline{A}_{kN}\underline{Y}\underline{B}_{11}\underline{A}_{Ni}\right)\underline{a}_i\right) + \underline{A}_{kN}\underline{Y}\left(\sum_{J=2}^{M}\underline{B}_{1J}\underline{a}_{N+J-1}\right)$$

$$\underline{b}_{l+N-1} = \underline{B}_{l1}\left(\sum_{i=1}^{N-1}\left(\underline{A}_{Ni} + \underline{A}_{NN}\underline{Y}\underline{B}_{11}\underline{A}_{Ni}\right)\underline{a}_i\right) + \left(\sum_{J=2}^{M}\left(\underline{B}_{l1}\underline{A}_{NN}\underline{Y}\underline{B}_{1J} + \underline{B}_{Lj}\right)\underline{a}_{N+J-1}\right) \qquad (7)$$

where $k = 1,2,3,\cdots,N-1$ and $l = 2,3,4,\cdots,M$. Note that relations (7) require only *one matrix inversion*:

$$\underline{Y} = \left(\underline{E} - \underline{B}_{11}\underline{A}_{NN}\right)^{-1}. \qquad (8)$$

A computer program was written using the preceding relations and utilizing the evolution strategy method (cf. [20], [22], [25], [26]) for optimizing the geometrical parameters for given specifications. Sufficient asymptotic behavior has been obtained by consideration of 14 TE_{1n}, TM_{1n}, and 43 TE_{m0} modes for the septate E-plane diplexer and triplexer configurations calculated in this paper. Convergence investigations by an additional inclusion of five higher order TE_{mn} and TM_{mn} modes of subsequent cutoff

wavenumbers show that these modes are negligible for an adequate distance between the E-plane and H-plane step discontinuities. Consideration of 45 TE_{m0} modes has turned out to be sufficient for the H-plane slit-coupled manifold types.

III. Design and Results

The computer-aided design is carried out in two steps by an optimization program which applies the evolution strategy method [20], [22], [25], [26]. In the first step, the individual filters are optimized according to the given specifications; these results are utilized for the initial values in the second step, which comprises the total multiplexer structure.

For the filter optimization in the first step (Fig. 5), an error function $F_{MS}(x)$ to be minimized is defined:

$$F_{MS}(\underline{x}) = \sum_{n=1}^{M_d} \left\{ \left\{ \left(20\log\left(\left| S_{21}(\underline{x}, f_{d_n}) \right| \right) - 1 \right) \cdot G_d \right\}^2 - G_d^2 \right\} + \sum_{m=1}^{M_s^{\mathrm{I}}} \left\{ \frac{a_s^{\mathrm{I}}}{20\log\left(\left| S_{21}(\underline{x}, f_{s_m}^{\mathrm{I}}) \right| \right)} \right\}^2 + \sum_{k=1}^{M_s^{\mathrm{II}}} \left\{ \frac{a_s^{\mathrm{II}}}{20\log\left(\left| S_{21}(\underline{x}, f_{s_k}^{\mathrm{II}}) \right| \right)} \right\}^2 \tag{9}$$

where

M_d = maximum frequency sample points in passband (about 5–10),

$M_s^{\mathrm{I,II}}$ = maximum frequency sample points in stopbands (about 5–10),

$\left. \begin{matrix} f_{d_i} \\ f_{s_i}^{\mathrm{I,II}} \end{matrix} \right\}$ = frequency sample points in passband and stopband,

$\underline{x}$ = parameter vector including the metal strip and resonator lengths of the filters to be optimized,

G_d = weighting factor (about 2–100),

$a_s^{\mathrm{I,II}}$ = desired stopband attenuation,

S_{21} = calculated transmission coefficient of the filter.

The results of the filter optimization for the examples presented in this paper are given in Tables I and II.

For the overall multiplexer optimization in the second step (Fig. 5(b)), the inclusion of the stopband behavior has turned out to be unnecessary. The error function $F(\underline{y})$ to be minimized, therefore, is based only on the most critical design criterion, the return loss behavior,

$$F(\underline{y}) = \sum_{n=1}^{M} \left\{ \frac{a_{r_n}}{20\log\left(\left| S_{11}(\underline{y}, f_n) \right| \right)} \right\}^2 \tag{10}$$

TABLE I
Computer-Optimized Dimensions (in mm) of the Metallic E-Plane Filters for the Ku-band Diplexer Examples

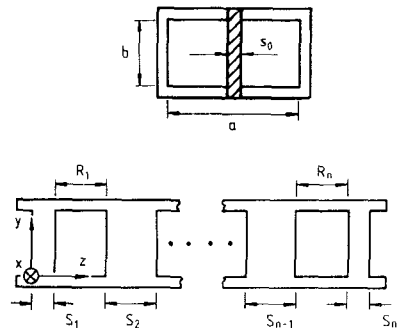

Ku - Band	Filter 3 5 resonators	Filter 4 5 resonators	Filter 1 7 resonators	Filter 2 7 resonators
Fig	8	8	7	7
S_0	0.190	0 190	0 190	0 190
$S_1 = S_n$	3 111	3.696	3 507	3.970
$S_2 = S_{n-1}$	9.979	11 519	10.971	11 987
$S_3 = S_{n-2}$	11 446	13 215	12.669	13 719
$S_4 = S_{n-3}$			13.034	14 082
$R_1 = R_n$	8 955	7 742	8.961	8 298
$R_2 = R_{n-1}$	8 968	7 717	8 971	8 293
$R_3 = R_{n-2}$	8.968	7 715	8.971	8.293
R_4			8 971	8.293

TABLE II
Computer-Optimized Dimensions (in mm) of the Metallic E-Plane Filters for the E-band Diplexers and Triplexers

E - Band	Filter 1 7 resonators	Filter 2 7 resonators	Filter 3 7 resonators
Fig	9,10	9,10	10
S_0	0 040	0 040	0.040
$S_1 = S_n$	0 731	0 780	0.873
$S_2 = S_{n-1}$	2 260	2.371	2 572
$S_3 = S_{n-2}$	2 601	2 729	2 936
$S_4 = S_{n-3}$	2 674	2.810	3.014
$R_1 = R_n$	1.854	1.741	1.638
$R_2 = R_{n-1}$	1 857	1 743	1 637
$R_3 = R_{n-2}$	1.857	1 743	1 637
R_4	1 857	1 743	1 637

where

M = maximum frequency sample points of all N passbands,

f_i = frequency sample points,

a_{r_i} = desired return loss,

$\underline{y}$ = parameter vector including the complete multiplexer dimensions to be optimized, such as (Fig. 1(a)) transformer section lengths and heights and spacing to the first filter segments.

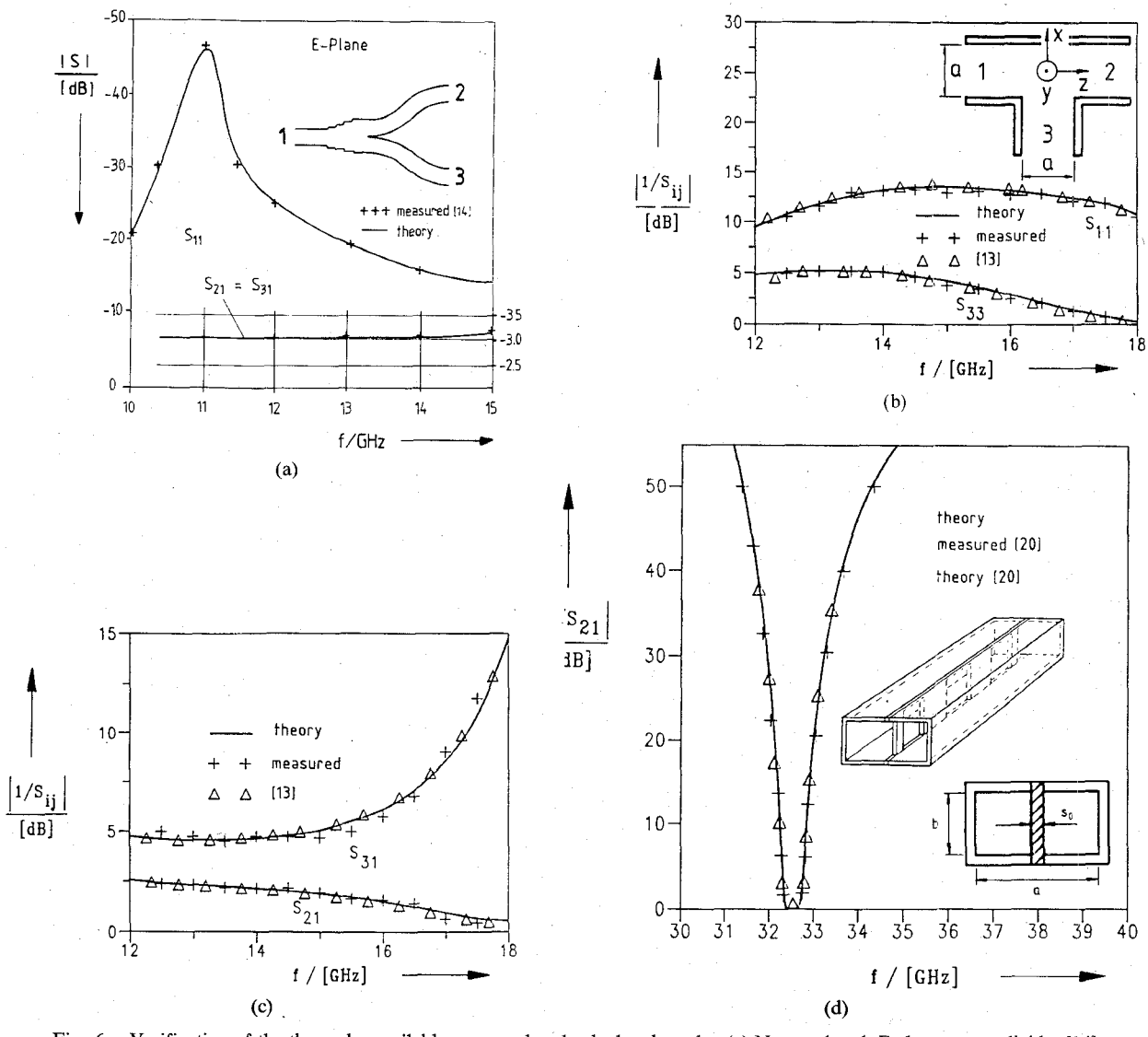

Fig. 6. Verification of the theory by available measured and calculated results. (a) Narrow-band E-plane power divider [14]. (b), (c) H-plane tee [13]. (d) Metal insert filter [20].

For a first verification of the theory, available measured results of some typical single components are considered. Fig. 6(a) compares the calculated scattering coefficients of a narrow-band E-plane bifurcation power divider with available measured data [14]. Very good agreement between measurements and theoretically predicted values is obtained. This holds also for the H-plane tee (Fig 6(b), and (c)) and the metal insert filter (Fig. 6(d)). For a second verification (Fig. 7), the insertion loss of the individual filters, indicated by the delta sign, is compared with the corresponding calculated overall scattering coefficients, between ports 1 and 2, and 1 and 3, respectively. The septate E-plane diplexer (Fig. 7(a)), and the H-plane slit-coupled manifold diplexer (Fig. 7(b)) demonstrate the very good agreement between the results.

To show the influence of the septum thickness on the diplexer characteristic, a computer-optimized Ku-band diplexer design example with two five-resonator metallic E-plane filters in the septate waveguide regions is presented in Fig. 8, for two septum thicknesses. Due to the inclusion of all relevant design parameters in the optimization process, only a one-step transformer is required to achieve the desired passband return loss of 26 dB. This holds nearly for greater septum thicknesses as well, as is shown by a design example with $t = 3$ mm (24 dB return loss).

For higher frequencies, a two-step transformer has been chosen, as is demonstrated by the E-band septate E-plane design example in Fig. 9(a). The common-port return loss of about 26 dB may nearly be achieved also by the manifold diplexer type (Fig. 9(b)). The efficiency of the design method described is demonstrated by the E-band triplexer design examples shown in Fig. 10(a) (septate E-plane type) and Fig. 10(b) (manifold H-plane slit-coupled type).

A comparison of the calculated with the measured overall insertion loss is shown for a septate E-plane diplexer realized in the waveguide Ku-band (Fig. 11). The measured minimum insertion loss is about 1 dB in both channels. The measured return loss (not shown here) was between 17

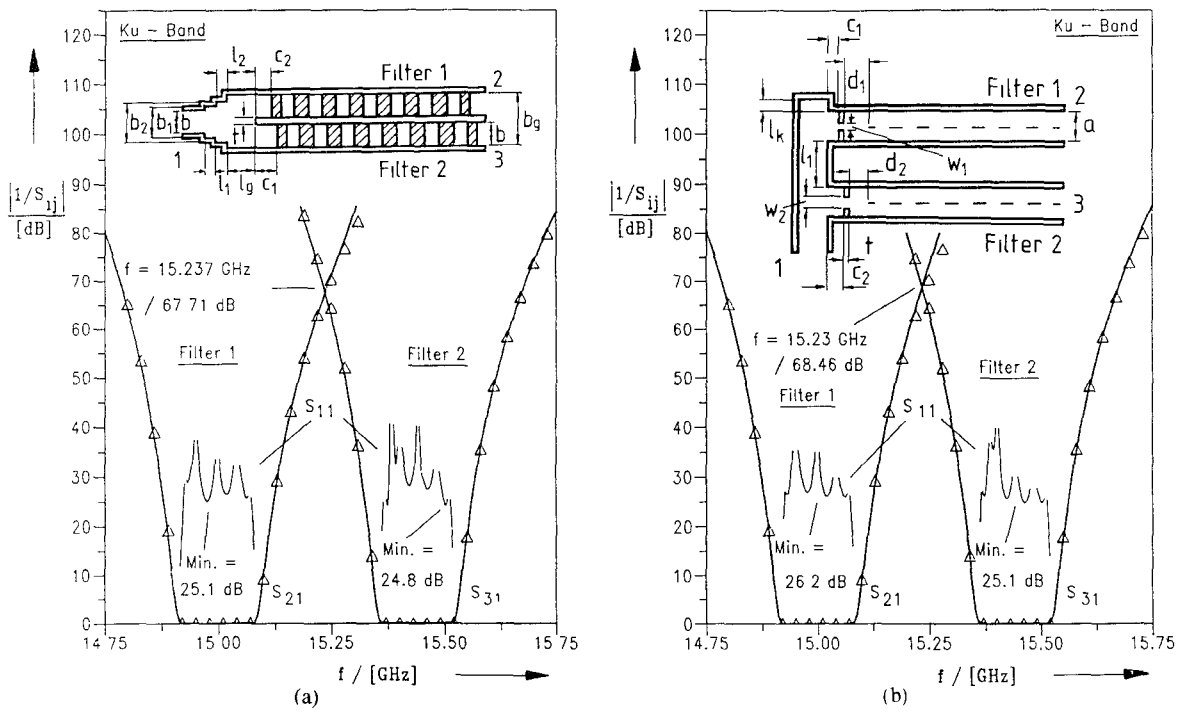

Fig. 7. Common-port scattering coefficients of *Ku*-band diplexers compared with the results of the single filter elements (ΔΔΔ). The filter dimensions are given in Table I.

(a) Septate *E*-plane type:
$a = 15.799$ mm, $b = 7.899$ mm, $t = 1$ mm, $b_g = 16.798$ mm
Filter 1: $f_{mitt} = 15$ GHz/$B/f_{mitt} = 0.012$
Filter 2: $f_{mitt} = 15.44$ GHz/$B/f_{mitt} = 0.0117$
$b_1 = 8.469$ mm, $l_1 = 5.544$ mm, $c_1 = 6.832$ mm
$b_2 = 12.932$ mm, $l_2 = 8.636$ mm, $c_2 = 7.820$ mm
$l_g = 16.212$ mm
(f_{mitt} = midband frequency; B/f_{mitt} = relative bandwidth).
(b) *H*-plane manifold type:
$a = 15.799$ mm, $b = 7.899$ mm, $t = 1$ mm
Filter 1: $f_{mitt} = 15$ GHz/$B/f_{mitt} = 0.012$
Filter 2: $f_{mitt} = 15.44$ GHz/$B/f_{mitt} = 0.0117$
$l_1 = 15.672$ mm, $w_1 = 11.911$ mm, $c_1 = 5.399$ mm, $d_1 = 22.671$ mm
$l_k = 0.052$ mm, $w_2 = 12.2$ mm, $c_2 = 2.871$ mm, $d_2 = 0.052$ mm.

and 32 dB for channel 1, and between 15 and 23 dB for channel 2. The deviations between theory and measurements are due to fabrication tolerances, which, for this first prototype example, are relatively high (up to 0.1 mm). The diplexer (Fig. 12) has been realized by using a milling machine for the waveguide housings; the filter resonators on the common metal sheet in the *E*-plane have been fabricated by metal-etching techniques.

IV. Conclusions

The modal *S*-matrix method described achieves a rigorous computer-aided design of two novel types of quasi-planar millimeter-wave multiplexers. Very compact designs are possible by using *E*-plane filters printed on a common metal sheet which is directly integrated in the septate sections of an *E*-plane trifurcated split-block waveguide housing. Further, the known useful principle of manifold multiplexers is extended to the case of millimeter-wave printed metallic *E*-plane filters. The optimization process takes all relevant influences into account, such as finite metallization thicknesses and higher order mode interactions at all discontinuities. As accurate and inexpensive metal-etching techniques may be utilized, the exact design theory permits high-performance, low-cost manufacturing of low-insertion-loss millimeter-wave multiplexers without the need for additional "trial-and-error" adjustment methods.

Appendix

A. Matrices $\underline{G}^{Lk}$ of Equation (3)

$$\underline{G}^{Lk} = \underline{D}^{YL}\underline{K}^{Lk}\underline{D}^{Zk}, \qquad k = \mathrm{I}, \mathrm{II}, \mathrm{III}, \cdots, M. \quad \text{(A1)}$$

Elements of the diagonal matrices $\underline{D}^{YL}, \underline{D}^{Zk}$:

$$D_i^{YL} = \sqrt{\frac{1}{Z^L_{h,e_i}}} = \begin{bmatrix} \sqrt{\dfrac{k_{zhi}}{\omega\mu}} \\ \sqrt{\dfrac{\omega\epsilon}{k_{zei}}} \end{bmatrix} \qquad D_i^{Zk} = \sqrt{Z^k_{h,e_i}}. \quad \text{(A2)}$$

$\underline{K}^{LK}$ are the coupling matrices of the *E*-plane and *H*-plane

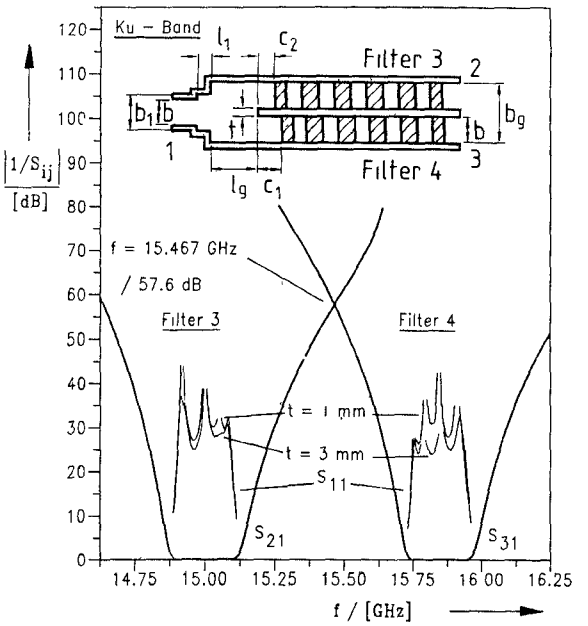

Fig. 8. Influence of the septum thickness on the diplexer characteristic. *Ku*-band septate *E*-plane diplexer example.

$a = 15.799$ mm, $b = 7.899$ mm
Filter 3: $f_{mitt} = 15$ GHz$/B/f_{mitt} = 0.017$,
Filter 4: $f_{mitt} = 15.85$ GHz$/B/f_{mitt} = 0.016$.
$t = 1$ mm: $b_g = 16.798$ mm
$b_1 = 14.887$ mm, $l_1 = 2.434$ mm, $c_1 = 9.074$ mm,
$l_g = 12.977$ mm, $c_2 = 8.285$ mm,
$t = 3$ mm: $b_g = 18.798$ mm
$b_1 = 14.464$ mm, $l_1 = 2.539$ mm, $c_1 = 7.291$ mm
$l_g = 14.621$ mm, $c_2 = 6.500$ mm.

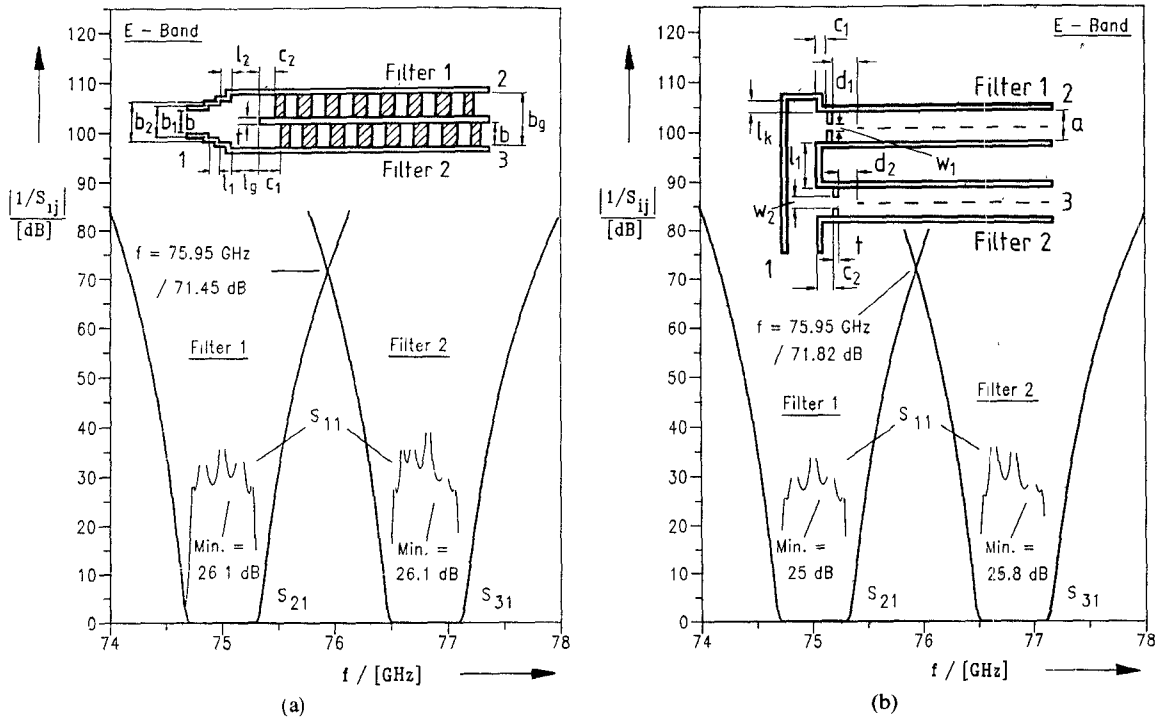

Fig. 9. Computer-optimized *E*-band diplexers.

(a) Septate *E*-plane type:
$a = 3.099$ mm, $b = 1.549$ mm, $t = 0.25$ mm, $b_g = 3.348$ mm
Filter 1: $f_{mitt} = 75$ GHz$/B/f_{mitt} = 0.00893$
Filter 2: $f_{mitt} = 76.8$ GHz$/B/f_{mitt} = 0.00872$
$b_1 = 1.662$ mm, $l_1 = 1.348$ mm, $c_1 = 1.560$ mm
$b_2 = 2.506$ mm, $l_2 = 0.126$ mm, $c_2 = 1.790$ mm
$l_g = 3.172$ mm.

(b) *H*-plane manifold type:
$a = 3.099$ mm, $b = 1.549$ mm, $t = 0.2$ mm
Filter 1: $f_{mitt} = 75$ GHz$/B/f_{mitt} = 0.0893$
Filter 2: $f_{mitt} = 76.8$ GHz$/B/f_{mitt} = 0.0872$
$l_1 = 3.214$ mm, $w_1 = 2.466$ mm, $c_1 = 0.934$ mm, $d_1 = 4.817$ mm
$l_k = 0.006$ mm, $w_2 = 2.408$ mm, $c_2 = 0.656$ mm, $d_2 = 0.009$ mm.

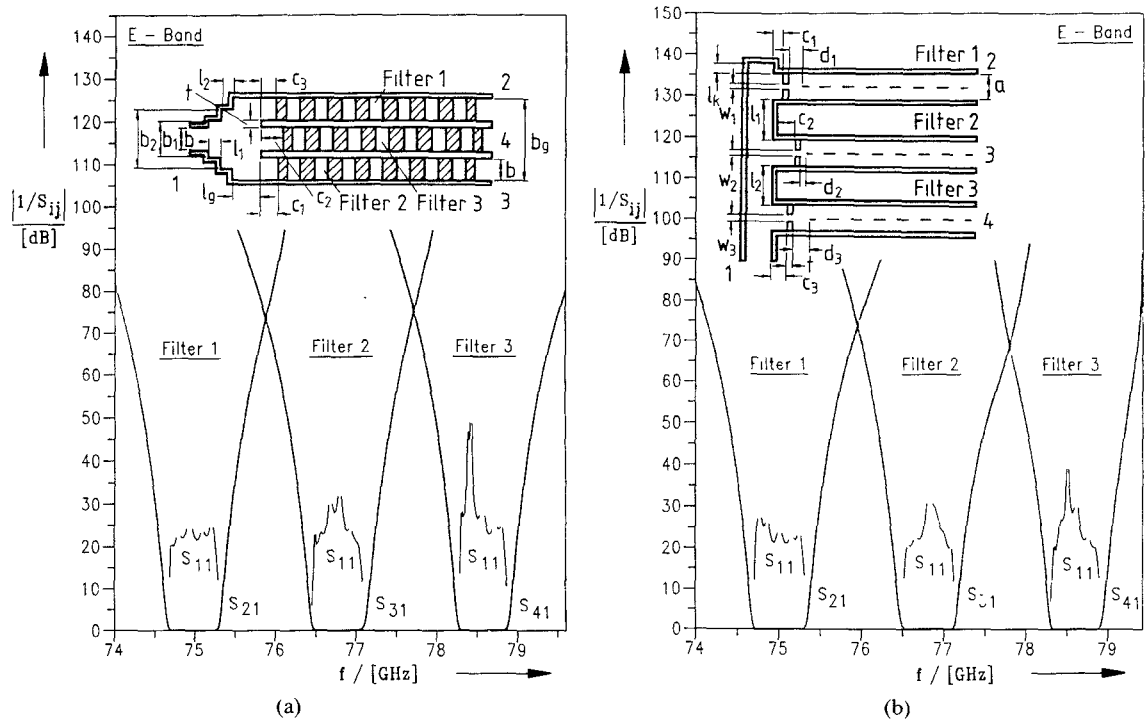

Fig. 10. Computer optimized *E*-band triplexers.

(a) Septate *E*-plane type:
$a = 3.099$ mm, b-1.549 mm, $t = 0.25$ mm, $b_g = 5.147$ mm
Filter 1: $f_{mitt} = 75$ GHz/$B/f_{mitt} = 0.00893$
Filter 2: $f_{mitt} = 76.8$ GHz/$B/f_{mitt} = 0.00872$
Filter 3: $f_{mitt} = 78.6$ GHz/$B/f_{mitt} = 0.00852$
$b_1 = 1.863$ mm, $l_1 = 3\,366$ mm, $c_1 = 0.865$ mm
$b_2 = 4.404$ mm, $l_2 = 1.672$ mm, $c_2 = 1.364$ mm
$l_g = 2.064$ mm, $c_3 = 1.097$ mm.

(b) *H*-plane manifold type:
$a = 3.099$ mm, $b = 1.549$ mm, $t = 0.2$ mm
Filter 1: $f_{mitt} = 75$ GHz/$B/f_{mitt} = 0\,0893$
Filter 2: $f_{mitt} = 76.8$ GHz/$B/f_{mitt} = 0.0872$
Filter 3: $f_{mitt} = 78.6$ GHz/$B/f_{mitt} = 0.0852$
$l_1 = 3.319$ mm, $w_1 = 2.306$ mm, $c_1 = 1.420$ mm, $d_1 = 4.500$ mm
$l_2 = 5.114$ mm, $w_2 = 2.277$ mm, $c_2 = 0.734$ mm, $d_2 = 0.010$ mm
$l_k = 0.005$ mm, $w_3 = 2.151$ mm, $c_3 = 2.967$ mm, $d_3 = 0.291$ mm.

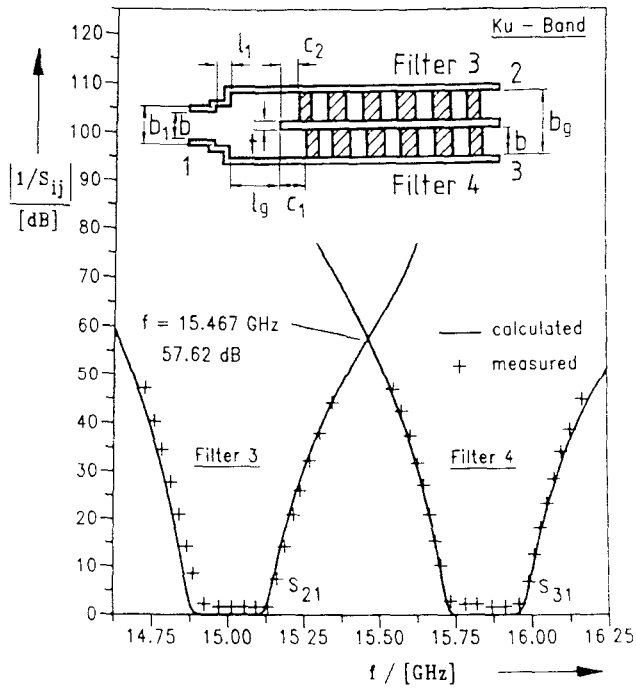

Fig. 11. Comparison of the calculated and measured overall insertion loss of a septate *E*-plane diplexer realized in the waveguide *Ku*-band.

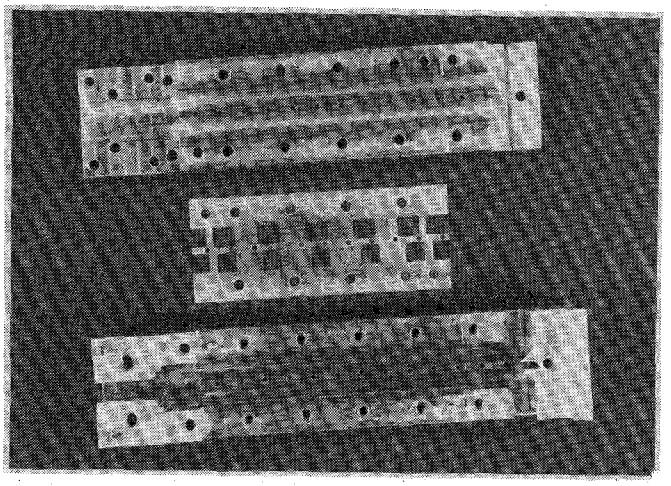

Fig. 12. Photograph of the fabricated septate E-plane diplexer.

n-furcation. The elements are given by

$$K_{ee_{ij}}^{Lk} = \left(\omega^2\mu\epsilon - k_{ze_i}^{L^2}\right)\int_{F_k} T_{e_i}^{L} T_{e_j}^{k}\, df \tag{A3}$$

$$K_{hh_{ij}}^{Lk} = \left(\omega^2\mu\epsilon - k_{zh_j}^{k^2}\right)\int_{F_k} T_{h_i}^{L} T_{h_j}^{k}\, df \tag{A4}$$

$$K_{eh_{ij}}^{Lk} = \oint_{R_k} T_{h_j}^{k}\, \text{grad}\, T_{e_i}^{L}\, d\vec{r} \tag{A5}$$

$$K_{he_{ij}}^{Lk} = \oint_{R_k} T_{h_i}^{L}\, \text{grad}\, T_{e_j}^{k}\, d\vec{r}. \tag{A6}$$

$T_{h,e_{i,j}}^{Lk}$ are the eigenfunctions, and $Z_{h,e}$ the wave impedances (A2) [23] of the subregions. F_k is the area of the subregion k, and R_k is the corresponding boundary.

B. Matrices of Equation (4)

$$\underline{M}_1 = -\underline{D}_1\underline{K}^{\text{II, III}}\underline{D}^{Y,\text{III}} + \underline{D}_2\underline{K}^{\text{I, III}}\underline{D}^{Y,\text{III}} \tag{A7}$$

$$\underline{M}_2 = \underline{D}_1\underline{D}^{Y,\text{I}} - \underline{D}_2\underline{D}^{Y,\text{I}}\underline{D}^{e\text{I}^{-1}} \tag{A8}$$

$$\underline{M}_3 = -\underline{D}_1\underline{D}^{Y,\text{I}}\underline{D}^{e\text{I}^{-1}} + \underline{D}_2\underline{D}^{Y,\text{I}} \tag{A9}$$

$$\underline{M}_4 = \underline{D}_1\underline{K}^{\text{I, III}}\underline{D}^{Y,\text{III}} - \underline{D}_2\underline{K}^{\text{II, III}}\underline{D}^{Y,\text{III}} \tag{A10}$$

$$\underline{N}_1 = \underline{Y}\left(-\underline{K}^{\text{III, I}}\underline{D}^{Y,\text{I}}\underline{M}_2 - \underline{K}^{\text{III, II}}\underline{D}^{Y,\text{I}}\underline{M}_3 - \underline{K}^{\text{III, I}}\underline{D}^{Y,\text{I}}\right) \tag{A11}$$

$$\underline{N}_2 = \underline{Y}\left(-\underline{K}^{\text{III, I}}\underline{D}^{Y,\text{I}}\underline{M}_3 - \underline{K}^{\text{III, II}}\underline{D}^{Y,\text{I}}\underline{M}_2 - \underline{K}^{\text{III, II}}\underline{D}^{Y,\text{I}}\right) \tag{A12}$$

$$\underline{N}_3 = \underline{Y}\left(-K^{\text{III, I}}\underline{D}^{Y,\text{I}}\underline{M}_1 - \underline{K}^{\text{III, II}}\underline{D}^{Y,\text{I}}\underline{M}_4 + \underline{D}^{Y,\text{III}}\underline{D}^{e\text{III}^{-1}}\right) \tag{A13}$$

$$\underline{Y} = \left(\underline{K}^{\text{III, I}}\underline{D}^{Y,\text{I}}\underline{M}_1 + \underline{K}^{\text{III, II}}\underline{D}^{Y,\text{I}}\underline{M}_4 - \underline{D}^{Y,\text{III}}\underline{D}^{e\text{III}}\right)^{-1}. \tag{A14}$$

$\underline{K}$ are the coupling matrices of the H-plane tee element (Fig. 3(d)). The elements of the matrices are given by

$$K_{ln}^{\text{I, III}} = \frac{\frac{n\pi}{2z_1}\frac{l\pi}{2x_1}}{\sqrt{z_1x_1}} \frac{\sin\left(k_{zhl}^{\text{I}}2z_1\right)}{k_{zhn}^{\text{III}}\left(\frac{l\pi}{2x_1}\right)^2 - k_{zhn}^{\text{III}^2}} \tag{A15}$$

$$K_{pn}^{\text{II, III}} = (-1)^n K_{ln}^{\text{I, III}} \tag{A16}$$

$$K_{nl}^{\text{III, I}} = \frac{\frac{l\pi}{2x_1}\frac{n\pi}{2z_1}}{\sqrt{z_1x_1}} \frac{\sin\left(k_{zhn}^{\text{III}}2x_1\right)}{k_{zhl}^{\text{I}}\left(\frac{n\pi}{2z_1}\right)^2 - k_{zhl}^{\text{I}^2}} \tag{A17}$$

$$K_{np}^{\text{III, II}} = -(-1)^n K_{nl}^{\text{III, I}}. \tag{A18}$$

The elements of the diagonal matrices $\underline{D}^{Y,\text{I}}$, $\underline{D}^{Y,\text{III}}$, $\underline{D}^{e\text{I}}$, and $\underline{D}^{e\text{III}}$ are given by

$$\underline{D}^{e\text{I}} = \begin{pmatrix} \ddots & & \\ & e^{jk_{zm}^{\text{I}}2z_1} & \\ & & \ddots \end{pmatrix}$$

$$\underline{D}^{e\text{III}} = \begin{pmatrix} \ddots & & \\ & e^{jk_{xm}^{\text{III}}2x_1} & \\ & & \ddots \end{pmatrix} \tag{A19}$$

$$D_i^{Y,\text{I}} = \sqrt{\frac{1}{Z_{h_i}^{\text{I}}}} \qquad D_i^{Y,\text{III}} = \sqrt{\frac{1}{Z_{h_i}^{\text{III}}}}. \tag{A20}$$

For diagonal matrices $\underline{D}_1$ and $\underline{D}_2$:

$$\underline{D}_1 = \underline{D}^{e\text{I}^{-1}}\underline{D}_2 \tag{A21}$$

$$\underline{D}_2 = \left(\underline{D}^{Y,\text{I}}\underline{D}^{e\text{I}}\right)^{-1}\left(\underline{E} - \underline{D}^{e\text{I}^{-1}}\underline{D}^{e\text{I}^{-1}}\right)^{-1}. \tag{A22}$$

C. Matrices $\underline{G}^{Lk}$ of Equation (6)

1) Case of TE_{m0} modes:

$$G^{Lk} = \underline{D}^{YL}\underline{K}_{hh}^{Lk}\underline{D}^{Zk} \qquad (k = \text{I, II}). \tag{A23}$$

Elements of the diagonal matrices $\underline{D}^{YL}$, $\underline{D}^{Zk}$:

$$D_i^{YL} = \sqrt{\frac{1}{Z_{h_i}^{L}}} = \sqrt{\frac{k_{zhi}}{\omega\mu}} \qquad D_i^{Zk} = \sqrt{Z_{h_i}^{k}}. \tag{A24}$$

$\underline{K}_{hh}^{Lk}$ are the coupling matrices of the single H-plane furcation given by (A4).

2) In the case of TE, TM mode excitation, the matrices $\underline{G}^{Lk}$ are given by relations (A1)–(A6).

References

[1] J. Reindel, "Printed WG circuits trim component costs," *Microwaves*, pp. 60–63, Oct. 1980.

[2] K. D. Breuer and N. Worontzoff, "Low cost multiplexer for channelized receiver front ends at millimeter waves," in *IEEE MTT-S Int. Symp. Dig.*, 1980, pp. 150–152.

[3] P. J. Meier *et al.*, "Channelized receiver covering 26 to 60 GHz with planar integrated-circuit elements," in *IEEE MTT-S Int. Symp. Dig.*, 1981, pp. 411–413.

[4] L. D. Cohen, N. Worontzoff, J. Levy, and A. Harvey, "Millimeter wave multiplexer with printed circuit elements for the 88 to 100 GHz frequency range," in *IEEE MTT-S Int. Symp. Dig.*, 1984, pp. 233–235.
[5] F. Arndt, J. Bronemann, D. Grauerholz, D. Fasold, and N. Schroeder, "Waveguide *E*-plane integrated-circuit diplexer," *Electron. Lett.*, vol. 21, pp. 615–617, 4th July 1985.
[6] C. Nguyen and K. Chang, "*W*-band wideband low loss planar integrated circuit diplexer," *Microwave J.*, pp. 157–161, July 1985.
[7] G. Reiter and T. Kolumban, "Diplexer arrangement utilizing an *E*-plane metal insert," in *Proc. 15th European Microwave Conf.* (Paris), Sept. 1985, pp. 859–864.
[8] P. J. Meier, "Integrated finline: The second decade," *Microwave J.*, vol. 28, pt. I: pp. 31–54, Nov. 1985; pt. II: pp. 30–48, Dec. 1985.
[9] Y.-C. Shih and T. Itoh, "Millimeter-wave diplexers with printed circuit elements," *IEEE Trans. Microwave Theory Tech.*, vol. MTT-33, pp. 1465–1469, Dec. 1985.
[10] Y.-C. Shih, L. Q Bui, and T. Itoh, "Mm-wave contiguous diplexer designed with printed circuit elements," *Microwave Syst. News*, vol. 17, pp. 46–53, Feb. 1987.
[11] G. L. Matthaei, L. Young. E. M. T. Jones, *Microwave Filters, Impedance-Matching Networks, and Coupling Structures*. New York: McGraw-Hill, 1964, ch. 13, 16.
[12] D. Rubin and A. R. Hislop, "Millimeter-wave coupled line filters," *Microwave J.*, pp. 67–78, Oct. 1980.
[13] W. Bräckelmann, "Hohlleiterverbindungen für Rechteck-hohlleiter," *Nachrichtentechnische Zeitschrift*, vol. 23, pp. 2–7, Jan. 1970.
[14] J. Dittloff, J. Bornemann, and F. Arndt, "Computer aided design of optimum *E*- or *H*-plane *n*-furcated waveguide power dividers," in *Proc. European Microwave Conf.* (Rome), Sept. 1987, pp. 181–186.
[15] J. L. Haine and J. D. Rhodes, "Direct design formulas for asymmetric bandpass channel diplexers," *IEEE Trans. Microwave Theory Tech.*, vol. MTT-25, pp. 807–814, Oct. 1977.
[16] J. D. Rhodes and R. Levy, "A generalized multiplexer theory," *IEEE Trans. Microwave Theory Tech.*, vol. MTT-27, pp. 99–111, Feb. 1979.
[17] J. D. Rhodes and R. Levy, "Design of general manifold multiplexers," *IEEE Trans. Microwave Theory Tech.*, vol. MTT-27, pp. 111–123, Feb. 1979.
[18] J. W. Bandler, S. Daijavad, and Q.-J. Zhang, "Exact simulation and sensitivity analysis of multiplexing networks," *IEEE Trans. Microwave Theory Tech.*, vol. MTT-34, pp. 93–101, Jan. 1986.
[19] Y. Konishi and K. Uenakada, "The design of a bandpass filter with inductive strip—Planar circuit mounted in waveguide," *IEEE Trans. Microwave Theory Tech.*, vol. MTT-22, pp. 869–873, Oct. 1974.
[20] R. Vahldieck, J. Bornemann, F. Arndt, and D. Grauerholz, "Optimized waveguide *E*-plane metal insert filters for millimeter-wave applications," *IEEE Trans. Microwave Theory Tech.*, vol. MTT-31, pp. 65–69, Jan. 1983.
[21] Y.-C. Shih and T. Itoh, "*E*-plane filters with finite-thickness septa," *IEEE Trans. Microwave Theory Tech.*, vol. MTT-31, pp. 1009–1013, Dec. 1983.
[22] F. Arndt *et al.*, "Modal *S*-matrix method for the optimum design of inductively direct-coupled cavity filters," *Proc. Inst. Elec. Eng.*,, vol. 133, pt. H, pp. 341–350, Oct. 1986.
[23] R. E. Collin, *Field Theory of Guided Waves*. New York: McGraw-Hill, 1960, ch. 5, 6, 8.
[24] H. Patzelt and F. Arndt, "Double-plane steps in rectangular waveguides and their applications for transformers, irises, and filters," *IEEE Trans. Microwave Theory Tech.*, vol. MTT–30, pp. 771–776, May 1982.
[25] F. Arndt, U. Tucholke, and T. Wriedt, "Computer-optimized multisection transformers between rectangular waveguides of adjacent frequency bands," *IEEE Trans. Microwave Theory Tech.*, vol. MTT-32, pp. 1479–1484, Nov. 1984.
[26] H. Schmiedel, "Anwendung der Evolutionsoptimierung bei Mikrowellenschaltungen," *Frequenz*, vol. 35, pp. 306–310, Nov. 1981.
[27] J. Dittloff and f. Arndt, "Rigorous design of septate *E*-plane multiplexers with printed circuit elements," in *IEEE MTT-S Int. Symp. Dig.*, May 1988, pp. 431–434.

✠

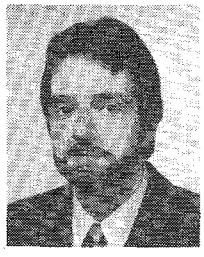

Joachim Dittloff was born in Rotenburg (Wümme), West Germany, on January 6, 1959. He received the Dipl.-Ing. and Dr.-Ing. degrees from the University of Bremen, West Germany, in 1984 and 1987, respectively, for research on microwave applications.

Since 1984 he has been with the Microwave Department of the University of Bremen. His work is on rectangular waveguide components (phase shifters, power dividers, multiplexing structures, and filters).

✠

Fritz Arndt (SM'83) received the Dipl.-Ing., Dr.-Ing., and Habilitation degrees from the Technical University of Darmstadt, Germany, in 1963, 1968, and 1972, respectively.

From 1963 to 1973, he worked on directional couplers and microstrip techniques at the Technical University of Darmstadt. Since 1972, he has been a Professor and Head of the Microwave Department at the University of Bremen, Germany. His research activities are in the area of the solution of field problems of waveguide, finline, and optical waveguide structures, of antenna design, and of scattering structures.

Dr. Arndt is a member of the VDE and NTG (Germany). He received the NTG award in 1970, the A. F. Bulgin Award (together with three coauthors) from the Institution of Radio and Electronic Engineers in 1983, and the best paper award of the Antenna Conference JINA 1986 (France).